Relationship Between Tropical Heating and Global Circulation: Interannual Variability

Huang-Hsiung Hsu

Department of Atmospheric Sciences
National Taiwan University

1. Introduction

The relationship between tropical heating and large-scale circulation has been one of the major topics in the study of general circulation both theoretically and empirically. Long-term averages of cloudiness distribution and estimated diabatic heating (e.g. Hoskins et al., 1989) suggest vigorous convection activity in the equatorial Africa, South America and western Pacific during the Northern Hemisphere winters. The configuration of stationary circulation in the tropics can be partly explained by the distribution of strong convection as suggested by Gill (1980). However, it is the temporal variation of these large-scale convection activity received more attention in recent years. The occurrence of El Niño/Southern Oscillation (ENSO) suggests a strong interannual variability of tropical convection and global circulation. The excessive heating added to the atmosphere during the El Niño years results in anomalous circulation pattern, especially in the tropics. Intraseasonal oscillation found by Madden and Julian (1972) adds complexity to the problem. The phenomenon is characterized by the shift of large-scale convective systems and corresponding circulations toward the east in the tropical western Pacific (Knutson and Weickmann, 1987).

In the past, most of the related studies focused on how tropical heating force large-scale circulation perturbations which in turn disperse energy in a manner similar to Rossby waves (Hoskins and Karoly, 1981). For example, the Pacific/North America pattern documented by Wallace and Gutzler (1981) are suggested to be forced by the tropical heating associated with ENSO (e.g. Horel and Wallace, 1981). However, similar pattern is also found in intraseasonal oscillation which exhibits strong tropical-extratropical interaction. The effect of extratropical perturbations on tropical convection has received much less attention than it deserves. Hsu and Lin (1992) in a study of global teleconnections suggested that the equatorial westerly regions, e.g. the eastern Pacific and Atlantic, in the upper troposphere are the preferred regions for inter-hemispheric interaction. Kiladas and Weickmann (1992) also found that the eastern Pacific is one of the regions where extratropical perturbations tend to induce tropical convection.

In this study, we applied a statistical technique called singular value decomposition following Bretherton et al. (1992) to objectively extract the most recurrent coupled mode between the global streamfunction and outgoing longwave radiation fields. This approach avoids the subjectivity in the study by Hsu and Lin (1992). The first

coupled mode appears to be of interannual time scale, and the second mode appears to be of intraseasonal time scale. Our results show the existence of a strong zonal-mean component in the both modes. The one associated with intraseasonal oscillation has received more attention recently. However, the zonal-mean component of interannual time scale which is evident in the composites of circulations associated with the ENSO (e.g. Yasunari, 1987) has been largely ignored. In this paper we shall discuss the results associated with interannual variability. The results associated with intraseasonal oscillation will be discussed in a following paper.

The data and analysis procedures are described in Section 2, and the statistical results are shown in Section 3. A global barotropic model was used to investigate the relationship between localized tropical divergence perturbations and the zonality of circulation perturbations. The results of numerical experiments and conclusions are presneted in Sections 4 and 5, recpectively.

2. Data and analysis procedures

The data used in this study are the ECMWF (European Centre for Medium-Range Weather Forecast) initialized wind data at 200 and 850 mb and outgoing longwave radiation at 12Z for the eight winters (defined as December, January, and February) from 1980/81 to 1987/88. The data are in a 5° × 5° degree grid globally for the wind fields and between 40°N and 40°S for the OLR. Streamfunctions at both 200 and 850 mb were computed by inverting Laplacian operator to the vorticity field. By doing that, we emphasize the rotaional flow. Changes of the both data assimilation system and forecast model at ECMWF in the past years have created artificial interannual variability in the processed data. The impact is most evident in the divergent wind field. We have thus chosen to use outgoing longwave radiation as a proxy variable to represent the variability of the irrotational flow in the tropics. Since the diabatic heating field is mainly balanced by the adiabatic cooling or heating due to vertical motion in the tropics, OLR is also used as a proxy variable representing the diabatic heating field.

Five-day running means were computed for the streamfunction and OLR fields to remove the high frequency variability. Singular value decomposition (SVD) analysis as described in Bretherton et al. (1992) was then applied to the temporal covariance matrix between the normalized streamfunction at 200 mb and OLR to retrieve the most recurrent coupled patterns. The data used for SVD analysis are in a 10° × 10° grid between 70°N and 70°S for the streamfunction and between 40°N and 40°S for the OLR. There are 524 and 324 points for the streamfunction and OLR fields, respectively. Since the emphasis of the study is on large-scale structure, the reduction in resolution does not affect our results. There are three major outputs of SVD analysis:

(1) Left and right singular vectors: Our results comprise 324 left and right vectors representing the spatial structure of coupled modes of streamfunction and OLR, respectively.

(2) Singular values: There are 324 singular values corresponding to 324 sets of singular vector in this study. Each singular value represents the amount of covariance explained by each mode. For SVD, however, squared covariance fraction (SCF) is more appropriate to represent the relative importance of each mode (Bretherton et al.,1992).

(3) Expansion coefficients: Time series of expansior coefficients represent the temporal variation of each left and right vectors. They are obtained by computing the inne product of the left and right vectors with the corresponding fields.

In this paper, left and right vectors derived directly from SVD analysis will not be shown. Instead, we shall present the correlation maps between the expansion coefficients of the OLR vectors and the OLR and streamfunction fields in the 5° × 5° resolution to show finer structure. They will be named homogeneous and heterogeneous correlation maps following the terminology used by Bretherton et al. (1992). By comparing these correlation maps, one can identify the spatial patterns in the OLR and streamfunction fields which are strongly coupled. Correlation statistics between the expansion coefficients of the OLR vectors and other variables such as the 850 mb streamfunction field will also be shown to illustrate the corresponding vertical structure and temporal variation.

3. Results of singular value decomposition

Fraction of total squared covariance explained by the first five sets of singular vectors, extracted from the OLR/200 mb streamfunction covariance matrix, are presented in Table 1. The first five modes explain 87.13 percent of total squared covariance. Among them the first mode alone explains 60.31 percent and, apparently, is the most prominent feature. The homogeneous and heterogeneous correlation maps between the expansion coefficients of the first OLR vector and the OLR and 200 mb streamfucntion fields are shown in Figures 1a and b , respectively. The correlation maps between the expansion coefficient of the first OLR vector and the 850 mb streamfunction fields is also shown in Figure 1c. A similar set of figures for the second coupled mode which explains 12.3 percent of total squared covariance is shown in Figure 2. To test the robustness of the coupled modes, SVD was also applied to the OLR/850 mb streamfunction covariance matrix and the 200/850 mb streamfunction covariance matrix. The first sets of singular vectors of the OLR/850 mb streamfunction and 200/850 mb streamfunction covariance matrices explain 40.9 and 61.8 percent of the total squared covariance, while the second sets of singular vectors of each matrix explain 17.1 and 11.2 percent, respectively. The corresponding homogeneous correlation maps are shown in Figure 3 for the first singular vectors and in Figure 4 for the second singular vectors. The first two coupled modes shown in Figures 1 and 2 are closely reproduced in the latter two analyses. It follows that the coupled modes are robust signals and the results are not affected by the choice of data combination. Empirical orthogonal function (EOF) analysis was also applied to the OLR, 200 and 850 mb streamfunction fields, respectively. The structures shown above all appear as the first two empirical orthogonal functions of the respective fields.

Time series of the expansion coefficients for the first two coupled modes are shown in Figure 5. Correlation coefficients between the expansion coefficients of OLR and 200 mb streamfunction fields are .87 and .88, respectively, as indicated in Table 1. The first coupled mode is characterized by a strong interannual variability similar to ENSO. In most of the winters except 1981/82 and 1985/86, the expansion coefficients tend to be either positive or negative. For example, 1982/83, 1986/87, 1987/88 are predominantly positive, while 1980/81, 1983/84, 1984/85 are predominantly negative. Subseasonal fluctuations are also evident. The second coupled mode are predominantly of intraseasonal time scale. To test the reproducibility of the modes discussed above, we repeated the SVD calculation after removing seasonal means for each winter. By doing that we were able to remove the first coupled mode shown here from the leading vectors. The second mode shown here becomes the first mode in the new calculation and is out-of-phase with the new second mode by one quarter of cycle in both space and time. In this paper, we shall focus on the first mode which exhibits interannual variability. The modes of intraseasonal time scale will be discussed in the following paper.

The OLR structure of the first coupled mode of the OLR/200 mb streamfunction covariance matrix (Figure 1a) exhibits positive correlation coefficients in the tropical Indian ocean/western Pacific and tropical South America, and negative correlation coefficients in the tropical central and eastern Pacific. A pattern of interannual time scale similar to the east-west dipole in the tropical Pacific in Figure 1a was also identified by Lau and Chan (1988) based on EOF analysis. The corresponding 200mb streamfunction structure (Figure 1b) shows an out of phase relationship between the streamfunction fields in the Northern and Southern Hemisphere. It indicates the existence of a strong zonal mean component. However, a dipole straddling the equator between the date line and 120W shows a reverse polarity.

A comparison between the OLR pattern in Figure 1a and the tight gradient along the equator in Figure 1b suggests that stronger-than-normal convection in the upper troposphere of the tropical central and eastern Pacific is accompanied by the westerly anomalies along the equator and at all longitudes except the region between the date line and 120°W where the easterly anomalies prevail. The Pacific jets in the both hemispheres are also strengthened and stretched because of the presence of the dipole in the tropical eastern Pacific. In the corresponding 850 mb streamfunction pattern (Figure 1c), a similar zonal-mean structure confined in higher latitudes is also evident. In the lower latitudes, however, a zonal wave one structure is the dominant feature. By comparing the 200 and 850 mb patterns, one finds an out-of-phase relationship in the lower latitudes and an in-phase relationship in the higher latitudes. Thus, in the tropics the westerly (easterly) anomalies in the upper troposphere are accompanied by the easterly (westerly) anomalies in the lower troposphere.

In order to illustrate the structure of the zonal-mean and eddy components more clearly, correlation coefficients between the expansion coefficient of the first OLR vector and the zonal-mean and eddy components of the 200 mb streamfunction fields are computed. The results are shown in Figure 6. The zonal-mean component (Figure 6b) clearly indicates an out-of-phase relationship between the two hemispheres. The values of correlation coefficients are about 0.8 and quite uniformly distributed poleward of 20 degree of latitudes. A sharp gradient between 20°N and 20°S is evident. This feature is consistent with the meridional variation of correlation coefficients between the expansion coefficient of the first OLR vector and the zonal-mean zonal wind shown in Figure 6c. The quadruple structure straddling the equator in the Pacific is the major feature of eddy components shown in Figure 6a. It consists of a pair of lows in the western Pacific and a pair of highs in the eastern Pacific. The dipoles of lows and highs are located at the poleward flank of the OLR pattern shown in Figure 1a. The features in the Southern Hemisphere are generally weaker than those in the Northern Hemisphere.

Lag correlation coefficients between the expansion coefficient of the first coupled mode and the 200 mb streamfunctions are presented in Figure 7. The results shows little time evolution between Day -20 and Day 20. Similar results are also obtained in the OLR and 850 mb streamfunction fields. The first coupled mode appears to be stationary.

The characteristics of the first coupled mode discussed above bear a close resemblance to the large-scale circulation and tropical convection associated with the ENSO (e.g. Yasunari, 1987). The results of SVD analysis reveal a strong relationship between tropical heating and large-scale circulation. Besides the dipolar circulation structure near the major tropical heating anomalies, there exist a zonal-mean component which exhibits an antisymmetric structure relative to the equator in the streamfunction fields and a symmetric structure in the height and wind fields. The existence of this mode is consistent with the concept of the ENSO. During the El Niño years,

excessive heatings occur in both the tropical atmosphere and the upper ocean in the Pacific. This results in positive height anomalies in the tropics and strengthening jet streams in the subtropics. Most of the studies by previous investigators focused on the wavy structure forced by the heating or sea surface temperature anomalies and have largely ignored the zonal-mean component which seems to be a strong signal associated with the fluctuation of ENSO events. The results shown here suggest that regional tropical heating effects (or convection) can lead to a change of both the zonal-mean and eddy components of global circulation.

4. Numerical experiments

The existence of the zonal-mean structure has been noticed in several empirical and theoretical studies. Hsu et al. (1989) in a study of 1985/86 intraseasonal oscillation prescribed a fixed heating of elliptic shape in a baroclinic model and were able to produce an antisymmetric zonal-mean streamfunction perturbation similar to that shown in Figure 1b. Similar results were also obtained by Hoskins and Jin (1993) in a study on the atmospheric responses to tropical heatings. Since the first coupled mode discussed in the preceeding section is mainly of interannual scale and stationary, the mode can be assumed to be in a quasi-steady state during a time span less than a season. Under this assumption, the corresponding heating and streamfunction perturbations should be in a quasi-balanced state.

Bearing this assumption in mind, we design a series of numerical experiments to investigate the relationship between the tropical convection and global circulation perturbations. The model is a T23 barotropic spectral model with Raleigh friction and biharmonic diffusion. The basic flow is the six-winter (1983/84 - 1988/89) means of the ECMWF 200 mb rotational fllow. A 'climatological' forcing was computed based on the basic flow and added in the model to balance the basic flow. Idealized divergences were then prescribed in the model to perturb the balanced flow. The global mean of the prescribed divergence is set to zero. The forcing specified in the model is the Rossby wave source suggested by Sardeshmukh and Hoskins (1988) which is defined as

$$-\nabla \cdot (\mathbf{V}'_{\chi} \bar{\varsigma}) \qquad (1)$$

where $\mathbf{V}'_{\chi}$ is the prescribed divergent wind and $\bar{\varsigma}$ is the mean absolute vorticity. The Rossby wave source includes not only the divergence term but also the advectional effect due to the divergent wind which could be important in the region of large vorticity gradient. Since the prescribed divergences are of small amplitudes compared with that of the basic flow, the behavior of the model is equivalent to that of a linear barotropic model. In every run, the response reached a quasi-steady state in first few days. When the model reaches steady state, the advectional effect due to the perturbations of rotational flows balances the prescribed forcing, i.e. the Rossby wave sources.

A series of experiments by prescribing divergence perturbation of elliptic shape at different location were carried out. Figure 8 shows the results of one of the experiments with the maximum of divergence at (5°S,160°W). The prescribed divergence, relative vorticity of the basic state, and the corresponding Rossby wave source is presented in Figures 8a,b,c, respectively. If only the direct effect of divergence (i.e. $-f(\nabla \cdot \mathbf{V}')$) were taken into account, the forcing should look like a dipole with a weaker minimum slightly north of the equator and a stronger maximum slightly south of the equator. The Rossby wave source presented in Figure 8c exhibits a much more complicated structure. The regions of minium and maximum values in the subtropics of the Northern and Southern Hemispheres, respectively, can be attributed to the vorticity advection by divergent flows in the vicinity of the Pacific jet streams where the gradient of relative vorticity is the largest. The Rossby wave source far away from tropical

forcing tends to be positive in the Northern Hemisphere and negative in the Southern Hemisphere. The responses of rotaional flow at Day 20 shown in Figure 8d are characterized by an out-of-phase relationship between the two hemispheres. In the vicinity of the forcing, there exist a pair of weak anticyclonic perturbations due to $-f(\nabla \cdot V')$. A wavy structure emanates from the tropical eastern Pacific, crosses North America and the Atlantic into the Indian Ocean.

Figures 9 and 10 show the results of two other experiments by placing the divergence pertubation at (5°S,0°E) and (5°S,160°W), respectively. Regions of minimum and maximum Rossby wave sources appear to the north and south of the tropical divergence. For the divergence perturbation centered at (5°S,0°E), the distribution of Rossby wave source exhibits a wavy structure over the Atlantic which is orthogonal to the distribution of the relative vorticity of the basic state (e.g. Figure 8b). By comparing Figures 8c and 10b, one notices in both cases a region of minimum Rossby wave source near the northern Pacific jet core where the gradient of relative vorticity is the largest. The similar distribution of minimum Rossby wave source in the subtropical Pacific in the both cases, as pointed out by Sardeshmukh and Hoskins (1988), demonstrates the remote effect of divergent flows and the insensitivity of atmospheric response to the location of tropical divergence. The far-field responses shown in Figures 9c and 10c, e.g. the out-of-phase relationship between the two hemispheres and the wavy structure described above, resemble that for the divergence perturbation centered at at (5°S,160°W) because of the similarity of the distribution of the far-field Rossby wave source.

We ran a series of experiments by placing prescribed divergence along the 5°S latitude for every 20 degrees of longitude. A pair of anticyclonic circulation tends to appear near the divergence perturbations for all cases, but its relative position to the prescribed divergence changes. Gill (1980) suggested that an anticyclonic pair should appear to the northwest and southwest of a tropical heating in a rest atmosphere because of the Sverdrup balance. The results of some of our experiments, e.g. for the divergence perturbations centered at (5°S,0°E) and (5°S,150°E), seem to agree with Gill's results, while some others did not. For example, the anticyclonic pair for the forcing at (5°S,160° W) appears to the north and south of the forcing. It is suggestive that in a more complicated basic state similar to the real atmosphere the distribution of Rossby wave source exhibits a complex structure and can not be balanced by the beta term alone as suggested by Gill (1980).

The results shown in Figures 8-10 are in a state in which the Rossby wave source is balanced by the vorticity advection by rotational flow. By comparing the distributions of the response and Rossby wave source (e.g. Figures 8c and d), one can observe the balance qualitatively. For example, the eastward flow near the Pacific jet core advects positive relative vorticity eastward to balance the large negative Rossby wave source. The wavy structure over the North America is organized in a manner so that the vorticity advection by rotational flows balance the wavy distribution of weak Rossby wave source in the same region. It is interesting to note that the wavy structure exists in all experiments and exhibits a configuration orthogonal to that of relative vorticity distribution. This result again demonstrates the remote effect of local divergence anomalies due to $-(V'_\chi \cdot \nabla \bar{\varsigma})$.

The zonal mean of Rossby wave source can be written as:

$$-\partial/\partial y\,[\,v'_\chi \bar{\varsigma}\,] = -\partial/\partial y\,([\,v'_\chi\,][\,\bar{\varsigma}\,] + [\,v'^*_\chi \bar{\varsigma}^*\,]) \qquad (2)$$

where bracket and asterisk represent zonal-mean and deviation from it, respectively. The first and second terms of

the right hand side are the contributions from zonal-mean and eddy components, respectively. The meridional distributions of the three terms in Equation 2 and the zonal-mean streamfunction perturbations corresponding to Figure 7 are presented in Figure 11. The zonal-mean streamfunction perturbations reach a quasi-steady state by Day 10 and indicates an out-of-phase relationship between the two hemispheres. The zonal-mean Rossby wave sources are negative and positive in the low latitudes of the Northern and Southern Hemispheres, respectively, and are in reversed signs in the higher latitudes. The contribution by eddies is much smaller than that of zonal-means. It follows that the flux due to the zonal-mean divergent wind is the dominant effect. The eddy term is important locally but plays a minor role in forcing zonal-mean response.

In order to mimic the observed outgoing longwave radiation pattern shown in the preceeding section, we prescribed a divergence/convergence dipole in the model with the centers at (5°S,120°E) and (5°S,160°W) as shown in Figure 12a. The divergence perturbations centered at (5°S,160°W) is twice as strong as the convergence perturbations centered at (5°S,120°E). It is intentional to specify different amplitudes for the two centers. Lau and Chan (1988) found that the largest interannual variability of the OLR occurs in the tropical central Pacific. Empirical studies of ENSO by previous investiagtors also indicate stronger than normal divergence in the tropical area during the El Niño years. The corresponding Rossby wave source and streamfunction response at Day 20 are shown in Figures 12b and c. The Rossby wave source again shows large amplitudes near the divergence perturbations and in the regions of sharp vorticity gradient. As in the previous experiments, the far-field responses tend to be negative in the Northern Hemisphere and positive in the Southern Hemisphere. The near-field response is dominated by a pair of anticyclonic circulation which exhibits reversed signs. A comparison of Figure 8d and 12c indicates that the major differences are the strengthened anticyclonic circulations near the forcing in the latter case.

The results shown above suggest the insensitivity of the response to the detailed structure of forcing. To investigate further, we prescribed the first OLR vector retrieved from SVD as divergence perturbations, but this time make the convergence twice as strong as the divergence. The results are shown in Figure 13. The Rossby wave source exhibits a complicated structure. The response is however very similar to that shown in Figure 12 except that the signs are reversed. The corresponding meridional distributions of the various terms of zonal-mean Rossby wave source are shown in Figure 14 and are similar to those in Figure 10. It again indicates weak contribution from the eddy term.

In the experiments reported here, we were able to simulate the observed global scale streamfunction perturbations, which exhibits an out-of-phase relationship between the Northern and Southern Hemispheres, by simply specifying an idealized divergence pattern in a barotropic model. Our simple experiments, however, have difficulties simulating detailed structures. The major discrepancies are found in the eastern part of the Northern Hemisphere, especially in the low latitudes. The first streamfunction vector (Figure 1) exhibits a pair of cyclonic circulation in the western Pacific when the convection in the central and eastern tropical Pacific is anomalously active. Our experiments fail to simulate this feature and the ridge right upstream of the pair of cyclonic circulation. Also, the zonal scale of the anticyclonic circulations (e.g. in Figure 13c) is too large compared to the results of SVD shown in Figure 1.

5. Conclusions

In this study, we applied singular value decomposition analysis to the OLR/200 mb streamfunction covariance matrix to retrieve the most recurrent coupled modes. The first and second modes explain 60.31 and 12.30 percent of total squared covariance, respectively. The first mode exhibits strong interannual variability, while the second mode is of intraseasonal time scale. In this paper, we emphasize the first mode and shall deal with the second mode in a separate paper. The characteristics of the first mode are listed as follows:

(1) A dipolar structure in the OLR field, with centers at (5°S,120°E) and (5°S,160°W), was found in the tropical Pacific.

(2) A zonal-mean structure in the 200 mb streamfunction field exhibits an out-of-phase relationship between the streamfunction perturbations in the Northern and Southern Hemispheres. The corresponding eddy components are characterized by a quadrupole straddling the equator in the Pacific with its centers to the north and south of the OLR dipole.

(3) Zonal wind fluctuations associated with the zonal-mean 200mb streamfunction perturbations exhibits a strong zonal-mean component near the equator.

(4) Zonality of the 850 mb streamfunction field is also evident in the high latitudes. However, the eddy components are the dominant features in the low latitudes and tend to be out of phase with those at 200 mb.

(5) The mode exhibits a strong interannual variability and appears to be stationary.

The most interesting feature above is the strong zonality of the streamfunction fields, especially at 200mb. It appears that the feature is strongly related to the activity in the tropical convection which exhibits little zonality. Similar characteristics are also found in the circulation fluctuations associated with ENSO (Yasunari, 1987) and is reflected in the expansion coefficients of the first coupled mode shown in Figure 5. It is also known that during the El Niño years there are more diabatic heating, mainly latent heat, in the tropical troposphere than in other years. The overall divergence in the upper troposphere of the tropics should also be stronger than normal. In order to investigate the effect of the divergence perturbation on the vorticity, we carried out a series of numerical experiments using a linearized barotropic spectral model by prescribing idealized divergence pattern at different locations. The corresponding Rossby wave source is prescribed as constant forcing and the model is integrated to a quasi-steady state. The results suggest that a localized divergence perturbation near the equator can force a zonal-mean component of streamfunction perturbation which exhibits a meridional structure with a node near the equator.

Our calcuations shows that the divergence of vorticity fluxes by zonal-mean divergent flows account for most of the Rossby wave source and the contributions from eddies are limited. The linearized equation of zonal-mean vorticity perturbation can be written as:

$$\partial/\partial t\,[\varsigma'] + \partial/\partial y\,([\bar{v}_\psi\,\varsigma'^*] + [v'^*_\psi\,\bar{\varsigma}^*]) = -\,\partial/\partial y\,([v'_\chi]\,[\bar{\varsigma}] + [v'^*_\chi\,\bar{\varsigma}^*]) \qquad (3)$$

by neglecting the terms associated with mean divergent flows. A positive zonal-mean Rossby wave source means an increase of vorticity and a tendency for negative streamfunction perturbation. By placing a divergence perturbation near the equator under the constraint of zero global-mean divergence, one finds a negative vorticity

tendency between the equator and 30°N and a positive vorticity tendency between 30°N and the north pole. A reversed polarity is found in the Southern Hemisphere. The corresponding streamfunction perturbations are negative in the Northern Hemisphere and positive in the Southern Hemisphere. The sharp gradient of vorticity tendency near the equator and the reversed polarity of the streamfunction perturbations in the two hemispheres suggest the existence of strong westerly perturbations near the equator. From the viewpoint of momentum balance, poleward transport of easterly momentum in the low latitudes will induce westerly perturbations near the equator.

Barotropic model seems to be able to simulate the zonality of the coupled mode but, not surprisingly, does a relatively poor job for the eddy component. The eddy component of the mode exhibits a baroclinic vertical structure in the low latitudes, e.g. a reversed polarity between the circulations in the upper and lower troposphere. Simulating such a structure is certainly beyond the capability of a barotropic model. At least, a baroclinic model is needed to include the thermodynamic effect which is likely crucial for a more successful simulation of the eddy component in the low latitudes.

Table I. The squared covariance explained by the first five modes. SCF and CSCF represent squared covariance fraction and cumulative squared covariance fraction, respectively; $r(a_k,b_k)$ is the temporal correlation coefficient between the expansion coefficients of the OLR and 200 mb streamfunction fields for the same mode.

k	SCF	CSCF	$r(a_k,b_k)$
1	60.31	60.31	0.87
2	12.30	72.61	0.88
3	8.67	81.28	0.81
4	3.51	84.79	0.89
5	2.34	87.13	0.83

References

Bretherton, C. S., C. S. Smith, and J. M. Wallace, 1992: An intercomparison of methods for finding coupled patterns in climate data. *J. Climate*, **5**, 541-560.

Gill, A. E., 1980: Some simple solutions for heat-induced tropical circulation. *Quart. J. Roy. Meteor. Soc.*, **106**, 447-462.

Horel, J. D: and J. M. Wallace, 1981: Planetary-scale atmospheric phenomena associated with the Southern Oscillation. *Mon. Wea. Rev.*, **109**, 813-829.

Hoskins, B. J., H.-H. Hsu, I. N. James, M. Masutani, P. D. Sardeshmukh, and G. H. White, 1989: Diagnostics of the global atmospheric circulation based on ECMWF analyses 1979-1989. World Meteorological Organization, WMO/TD-No. 326, 217 pp.

Hoskins, B. J. and D. J. Karoly, 1981: The steady linear response of a spherical atmosphere to thermal and orographic forcing. *J. Atmos. Sci.*, **38**, 1179-1196.

Hsu, H.-H., B. J. Hoskins, and F.-F. Jin, 1990: The intraseasonal oscillation and the role of the extratropics. J. Atmos. Sci., **47**, 823-839.

Hsu, H.-H. and S.-H. Lin, 1992: Global teleconnections in the 250-mb streamfunction field during the Northern Hemishpere winter. *Mon. Wea. Rev.*, **120**, 1169-1190.

Kiladis, G. N. and K. M. Weickmann, 1992: Extratropical forcing of tropical Pacific convection during Northern winter. *Mon. Wea. Rev.*, **120**, 1924-1938.

Knutson, T. R. and K. M. Weickmann, 1987: 30-60 Day atmospheric oscillations: Composite life cycles of convection and circulation anomalies. *Mon. Wea. Rev.*, **115**, 1407-1436.

Lau, K.-M. and P. H. Chan, 1988: Intraseaonal and interannual variations of tropical convection: A possible link between the 40-50 day oscillation and ENSO? *J. Atmos. Sci.*, **45**, 506-521.

Madden, R. A. and P. R. Julian, 1972: Description of global-scale circulation cells in the tropics with a 40-50 day period. *J. Atmos. Sci.*, **29**, 1109-1123.

Sardeshmukh, P. D. and B. J. Hoskins, 1988: The generation of global rotational flow by steady idealized tropical divergence. *J. Atmos. Sci.*, **45**, 1228- 1251.

Wallace, J. M. and D. S. Gutzler, 1981: Teleconnections in the geopotential height field during the Northern Hemisphere winter. Mon. Wea. Rev., **109**, 784-812.

Yasunari, T., 1987: Global structure of the El Niño/Southern Oscillation. Part I. El Nino composites. *J. Meteor. Soc. Japan*, **65**, 67- 80.

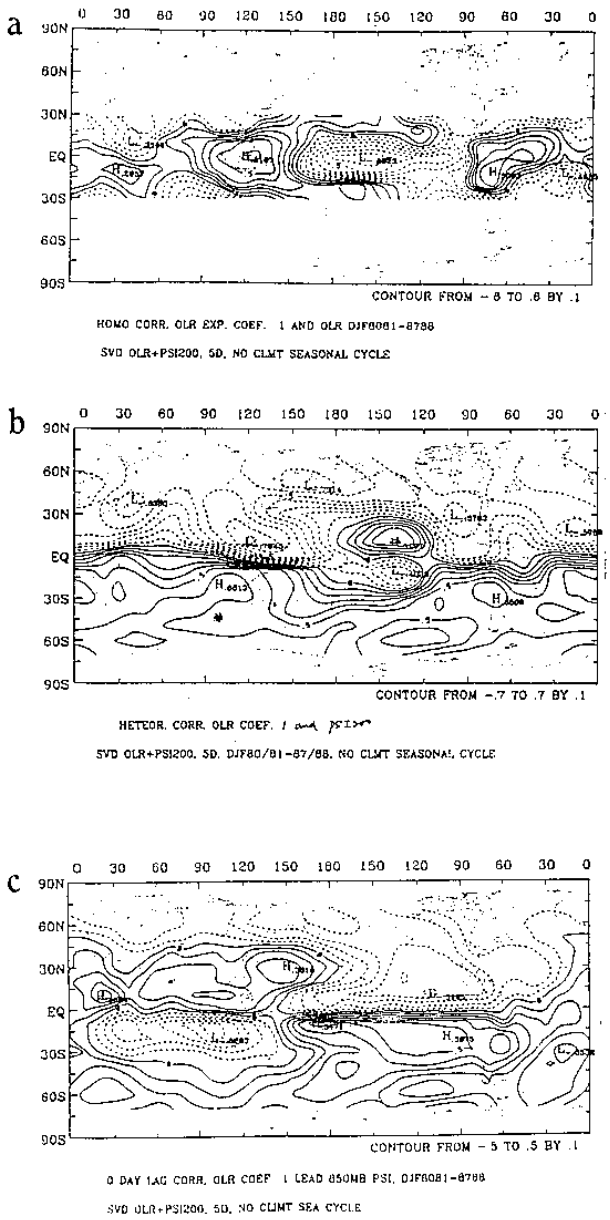

Figure 1. Correlation maps between the expansion coefficient of the first OLR vector, which is extracted from the OLR/200 mb streamfunction covariance matrix, with the (a) OLR, (b) 200 mb streamfunction, and (c) 850 mb streamfunction fields. Contour interval is 0.1.

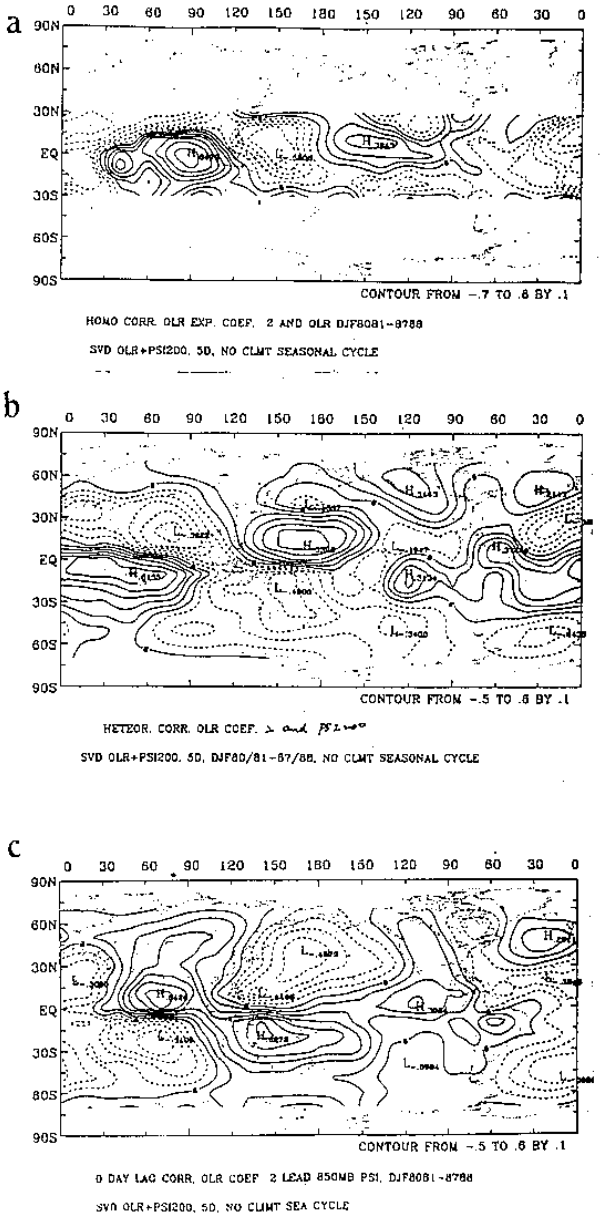

Figure 2. Correlation maps between the expansion coefficient of the second OLR vector, which is extracted from the OLR/200 mb streamfunction covariance matrix, with the (a) OLR, (b) 200 mb stramfunction, and (c) 850 mb streamfunction fields. Contour interval is 0.1.

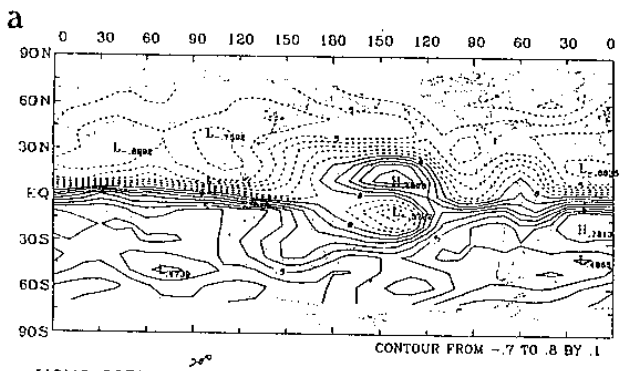

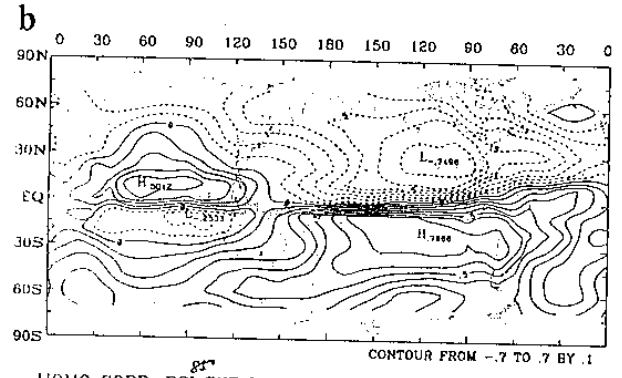

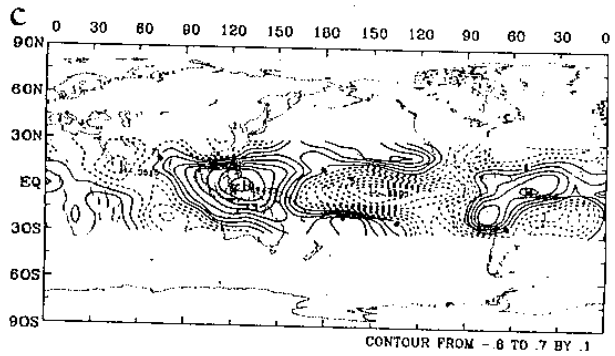

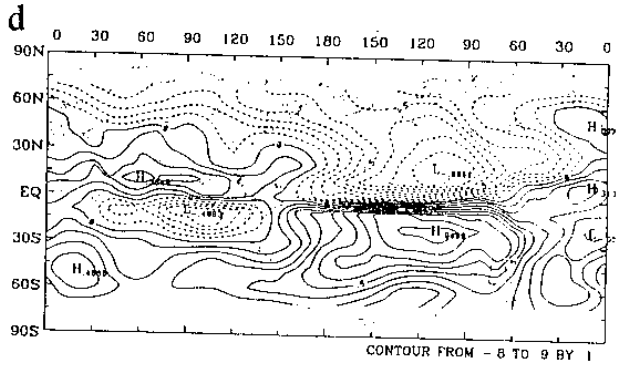

Figure 3. Homogeneous correlation maps of the first mode extracted from the 200/850 mb streamfunction covariance matrix for the (a) 200 mb and (b) 850 mb streamfunction fields, respectively; and from the OLR/850 mb streamfunction covariance matrix for the (c) OLR and (d) 850 mb streamfunction fields, respectively. Contour interval is 0.1.

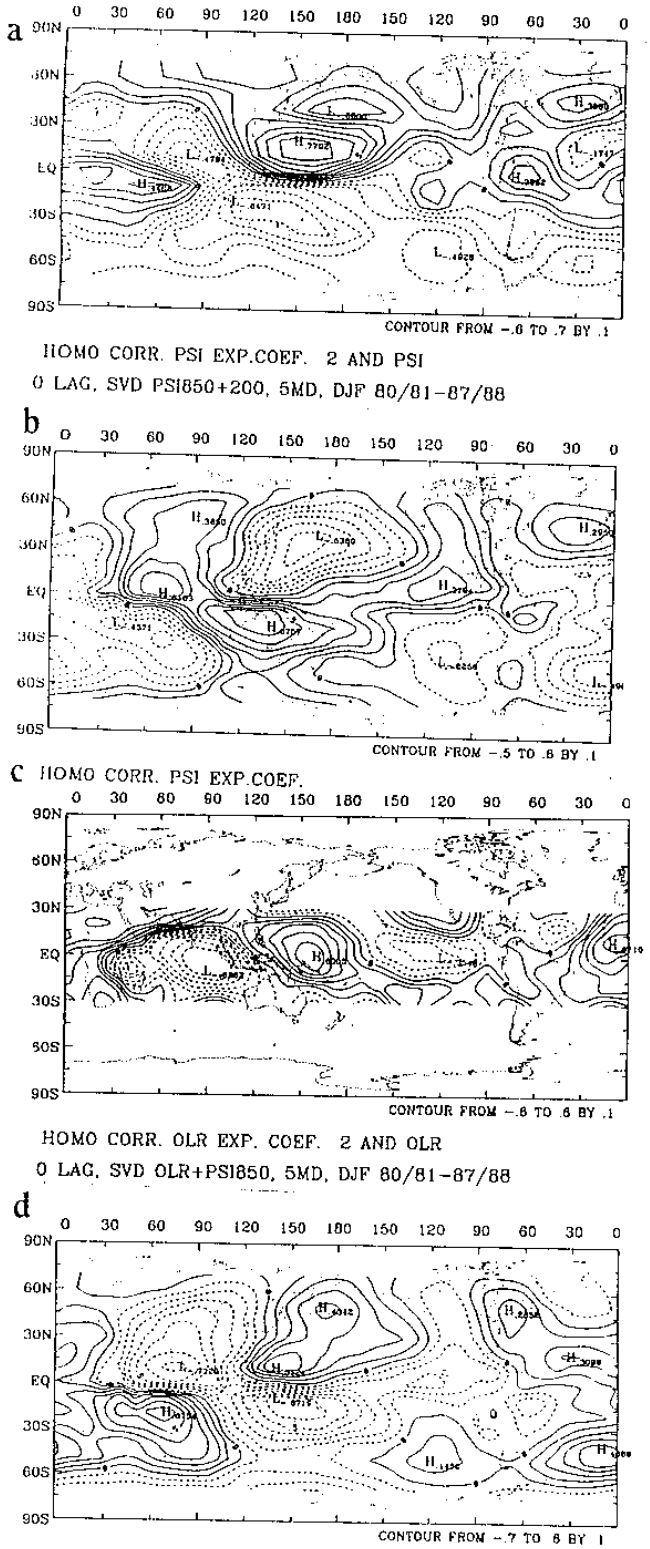

Figure 4. Homogeneous correlation maps of the second mode extracted from the 200/850 mb streamfunction covariance matrix for the (a) 200 mb and (b) 850 mb streamfunction fields, respectively; and from the OLR/850 mb streamfunction covariance matrix for the (c) OLR and (d) 850 mb streamfunction fields, respectively. Contour interval is 0.1.

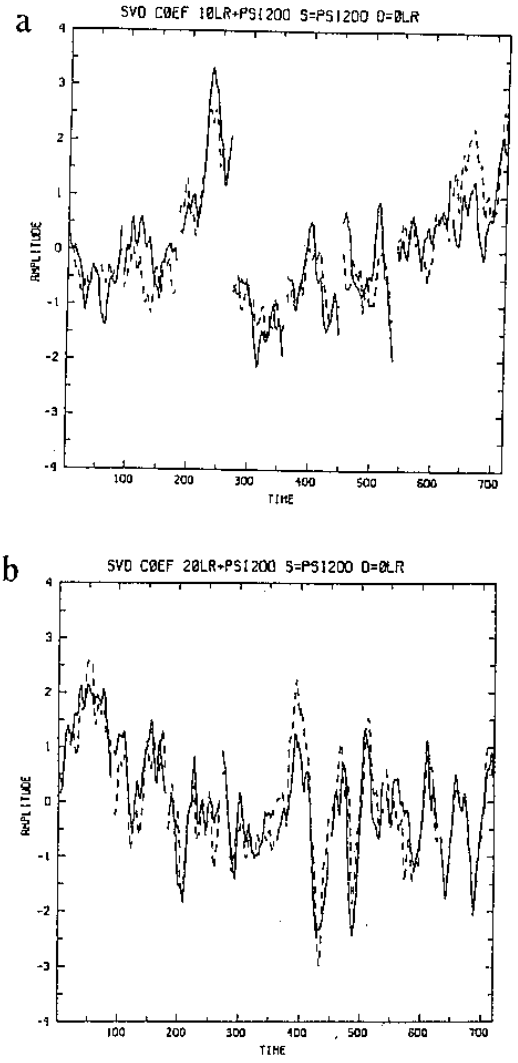

Figure 5. Normalized expansion coefficients of the (a) first and (b) second mode. Dashed and solid lines are for the OLR and 200 mb streamfunction fields, respectively.

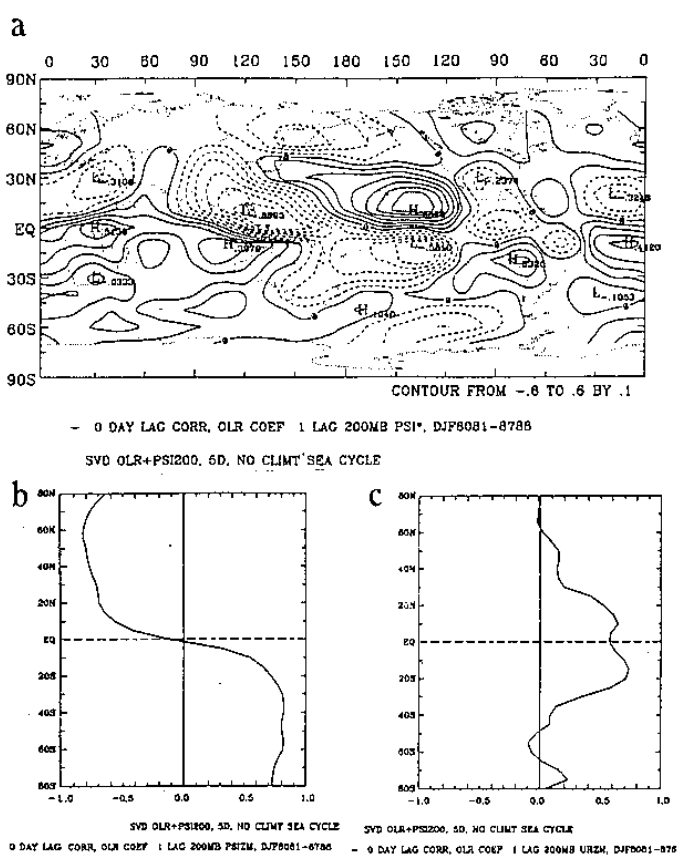

Figure 6. Correlation maps between the expansion coefficient of the first OLR vector with the (a) eddy streamfunction, (b) zonal-mean streamfunction, and (c) zonal-mean zonal wind fields at 200mb. Contour interval in (a) is 0.1.

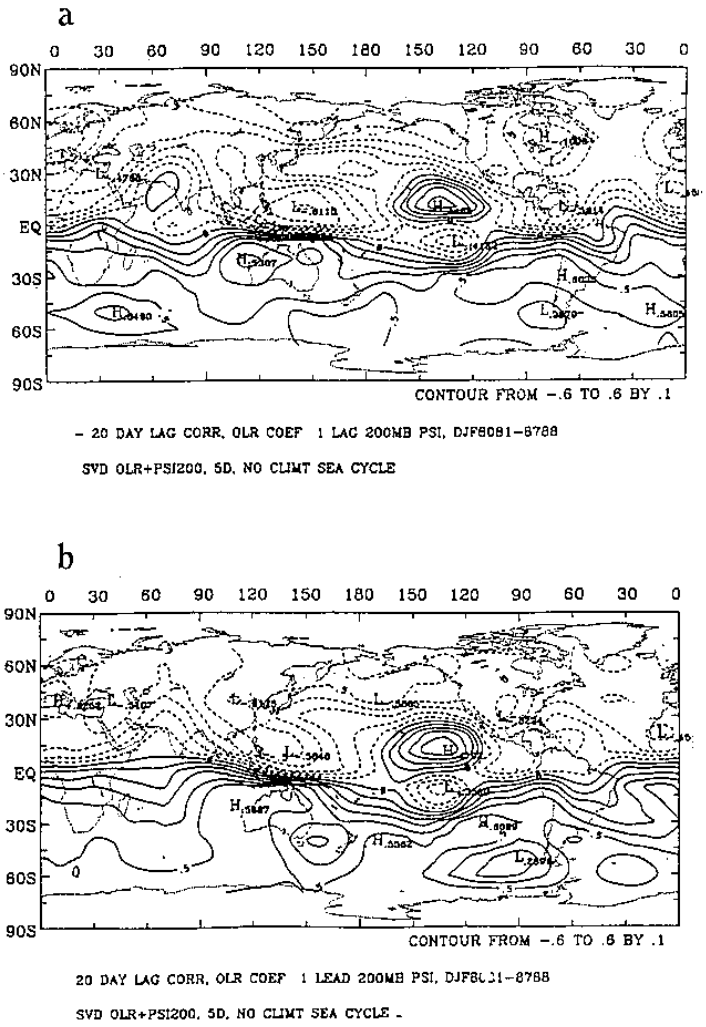

Figure 7. Lag correlation maps between the expansion coefficient of the first OLR vector with the 200 mb streamfunction field (a) 20 days before and (b) 20 days after. Contour interval is 0.1.

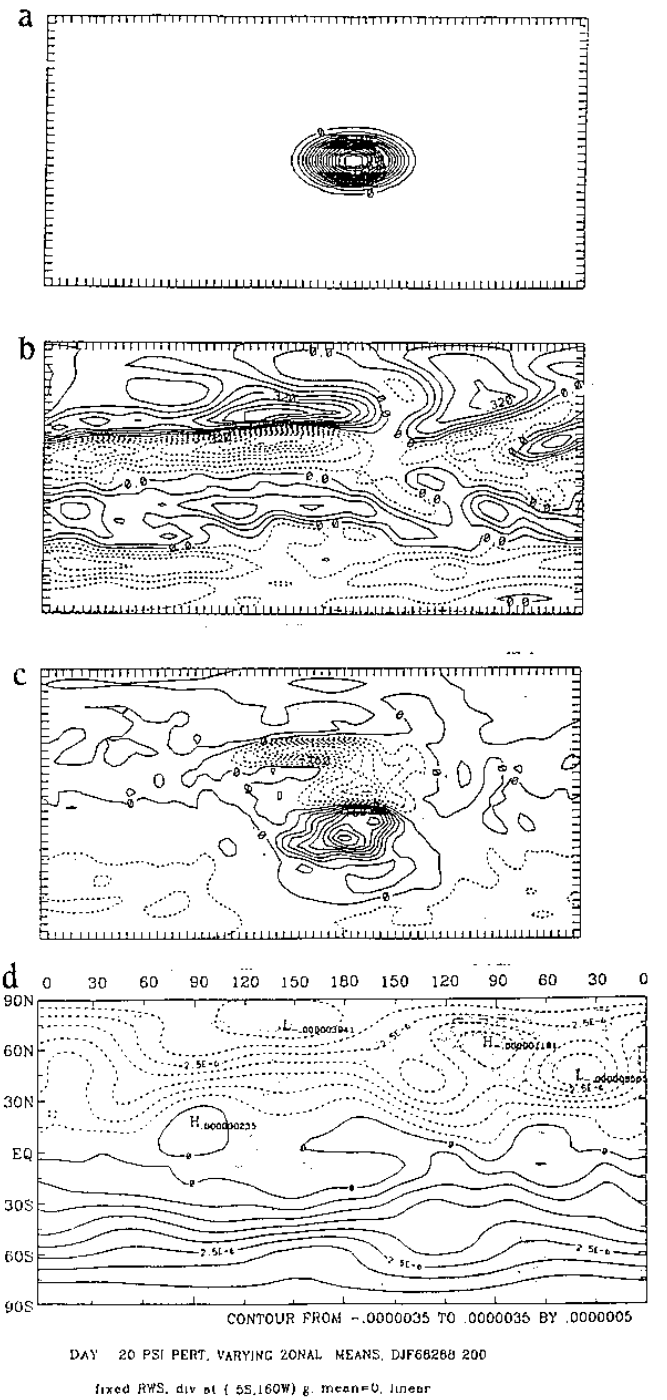

Figure 8. Results of numerical experiment using a T23 global barotropic model: (a) Prescribed divergence perturbations of elliptic shape with the center at (5°S,160°W), (b) relative vorticity field of the basic state, (c) Rossby wave source, (d) streamfunction perturbations by Day 20.

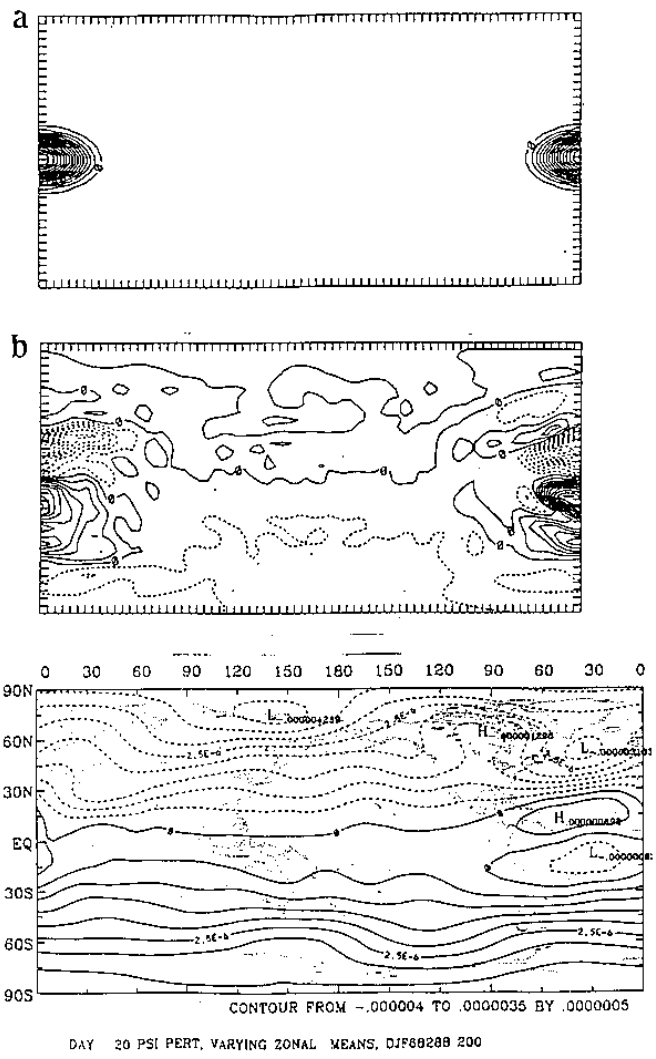

Figure 9. Results of numerical experiment using a T23 global barotropic model: (a) Prescribed divergence perturbations of elliptic shape with the center at (5°S,0°E), (b) Rossby wave source, (c) streamfunction perturbations by Day 20.

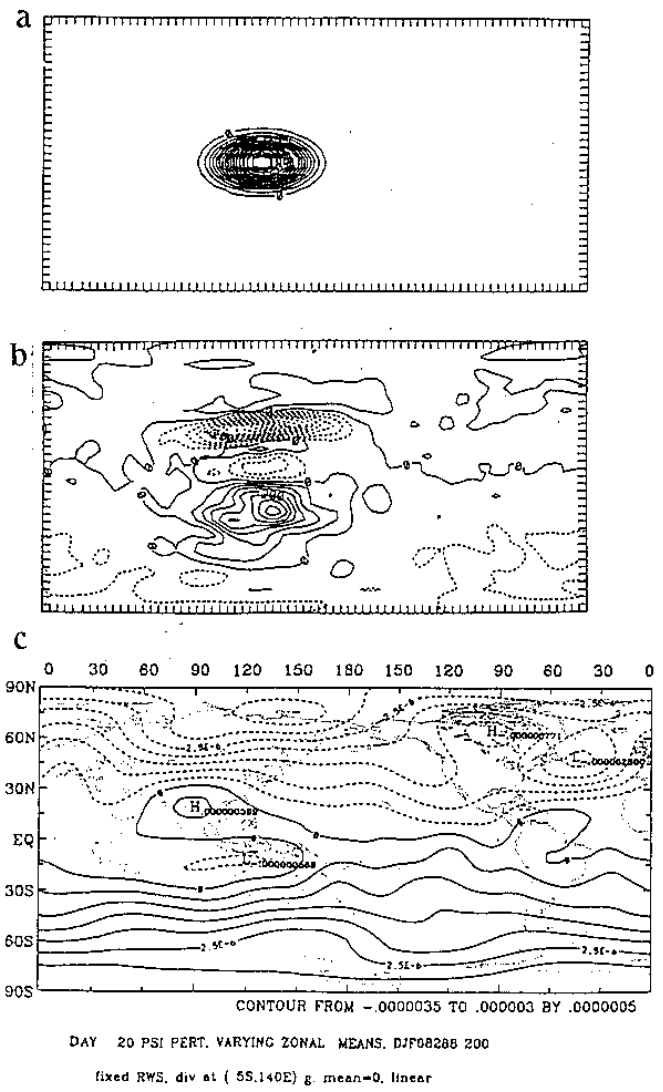

Figure 10. Results of numerical experiment using a T23 global barotropic model: (a) Prescribed divergence perturbations of elliptic shape with the center at (5°S,150°E), (b) Rossby wave source, (c) streamfunction perturbations by Day 20.

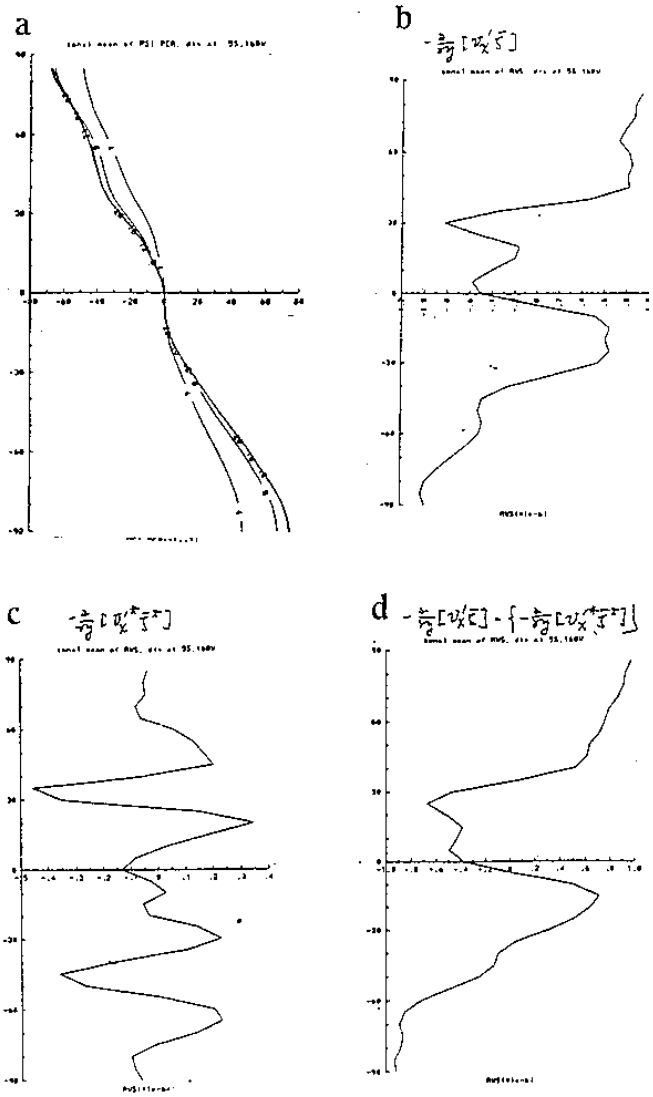

Figure 11. (a) Meridional distribution of the zonal-mean streamfunction perturbations for every 4 days in the experiment shown in Figure 8; and meridional distributions of various terms of Rossby wave source (b) $-\partial/\partial y\,[\,v'_\chi\,\zeta\,]$, (c) $-\partial/\partial y\,[\,v'^*_\chi\,\zeta^*\,]$, and (d) $-\partial/\partial y\,(\,[\,v'_\chi\,]\,[\,\zeta\,]\,)$. Note that the abscissa is ticked every 0.2 in (b) and (d), and 0.1 in (c).

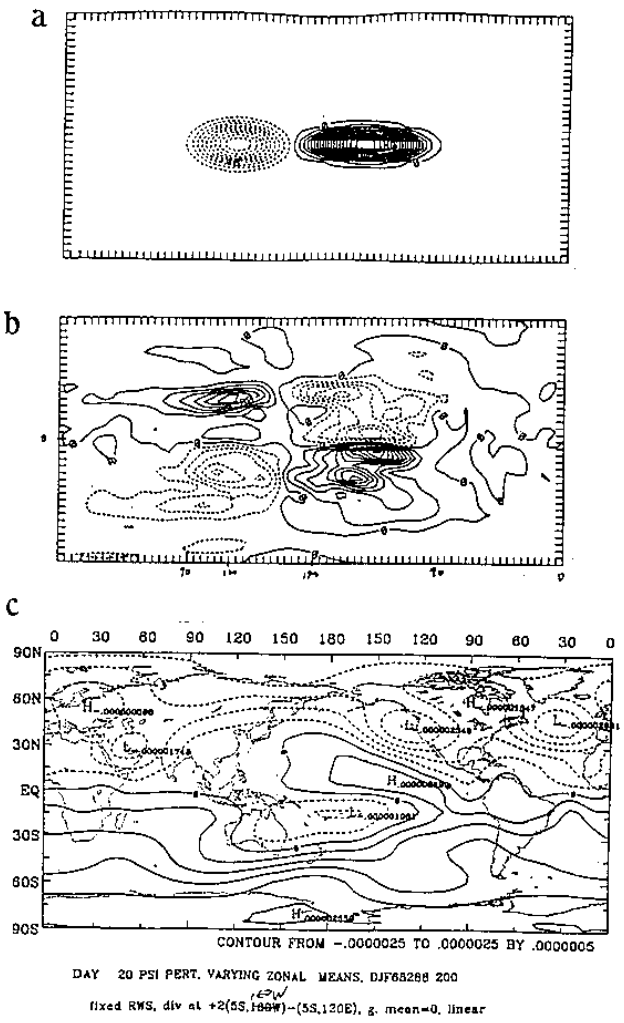

Figure 12. Results of numerical experiment using a T23 global barotropic model: (a) prescribed dipole of divergence perturbations of elliptic shape with the centers at (5°S,160°W) and (5°S,150°E), (b) Rossby wave source, (c) streamfunction perturbations by Day 20.

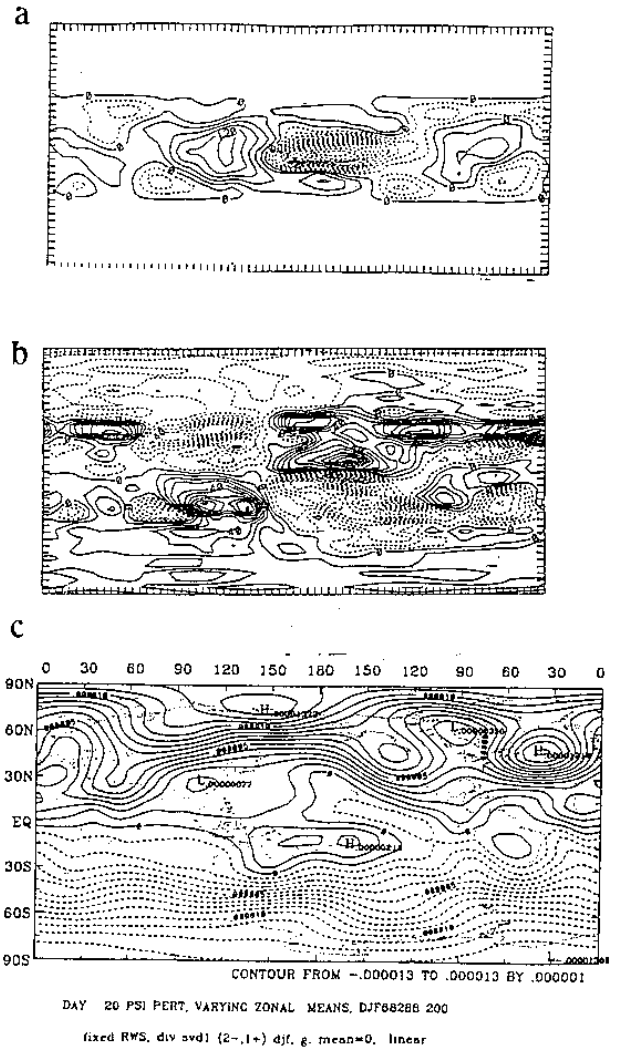

Figure 13. Results of numerical experiment using a T23 global barotropic model: (a) prescribed divergence pattern mimicking the first OLR vector in Figure 1, but with the convergence twice as strong as the divergence, (b) Rossby wave source, (c) streamfunction perturbations by Day 20.

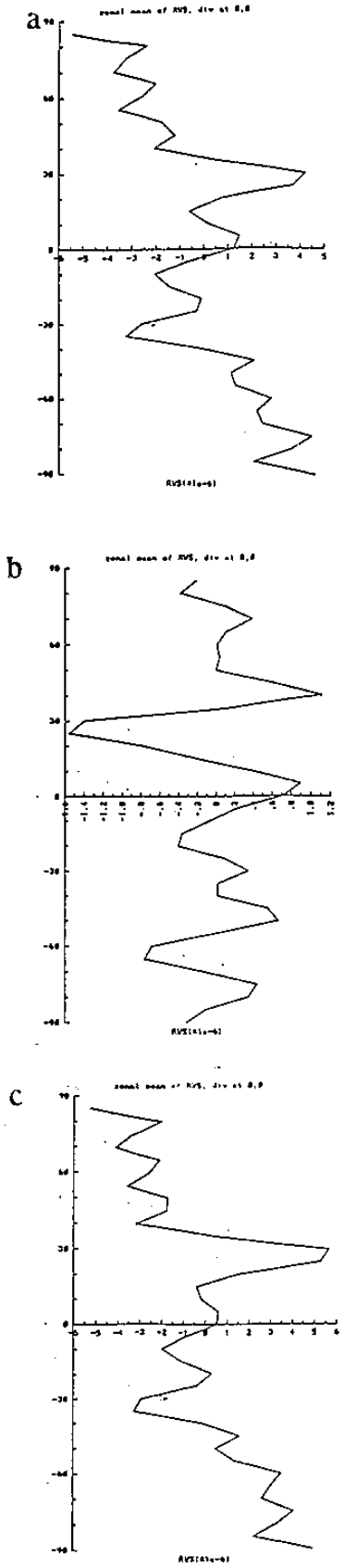

Figure 14. (a,b,c) Same as in Figure 12 (b,c,d) but for the experiment shown in Figure 13.

熱帶熱源與全球環流的關係：年際變化

許晃雄
國立台灣大學大氣科學系

摘　　要

本研究利用奇值分解法及數值模擬探討熱帶對流與對流層內全球環流之間的關係。

首先，我們利用奇值分解法自200毫巴流函數/出長波輻射協方差矩陣導出最重要的偶合模。第一個偶合模的流函數向量呈現南-北半球反相位的型式及在赤道附近的高梯度。因此，此模將引起緯向平均緯流的擾動。出長波輻射向量則呈現偶極結構：一個中心在南緯5度，東經150度；另一中心在南緯5度，西經160度。此模的變化，以年際變化最大，而且與艾尼紐/南方振盪有關。比如，正相位通常出現於艾尼紐年，負相位則出現於反艾尼紐年。

我們進一步設計一系列數值模擬，將理想化的輻散場沿著南緯5度植於全球正壓波譜模式，探討模式流函數場的反應。模式所用基本場爲歐洲中期天氣預報中心的ECMWF 200毫巴氣候平均風場。理想輻散場所引起的羅士培波源則作爲強迫作用。當模式達到準恆定狀態，其流函數擾動場亦呈現南-北半球反相位的結構，與第一個偶合模式類似。模式的反應顯然對理想輻散場位置不敏感，只要產生類似的緯向平均強迫作用，就會呈現南-北半球反相位的結構。